*Progress In Electromagnetics Research C, Vol. 32, 123–137, 2012*

# IMPROVING CCD PERFORMANCE BY THE USE OF LOCAL FRINGE FREQUENCIES

**A. Bouaraba[1, *], D. Borghys[2], A. Belhadj-Aissa[3], M. Acheroy[2], and D. Closson[2]**

[1]Ecole Militaire Polytechnique, Bordj el Bahri, BP 17, Algiers, Algeria

[2]Royal Military Academy, Avenue de la Renaissance 30, Brussels 1000, Belgium

[3]University of Sciences and Technology Houari Boumedienne, El Alia, BP 32, Bab Ezzouar, Algiers, Algeria

**Abstract**—Coherent Change Detection (CCD) using multi-temporal Synthetic Aperture Radar (SAR) is one of the most important applications of remote sensing technology. With the advent of high-resolution SAR images, CCD has received a lot of attention. In CCD, the interferometric coherence between two SAR images is evaluated and analyzed to detect surface changes. Unfortunately, the sample coherence estimator is biased, especially for low-coherence values. The consequence of this bias is the apparition of highly coherent pixels inside the changed area. Within this context, the detection performance will considerably degrade, particularly when using high resolution SAR data. In this paper, we propose a new CCD method based on cleaning of coherence inside changed areas, which is characterized by high Local Fringe Frequencies (LFF) values, followed by a space-averaged coherence method. According to the proposed method, the results obtained with Cosmo-SkyMed (CSK) SAR data show an enhancement of change detection performance of about 6% while preserving subtle changes.

## 1. INTRODUCTION

Change detection with remote sensing SAR images involves a pair of co-registered images acquired over the same area at different times [1]. To identify changes, different methods are commonly

*Received 3 July 2012, Accepted 20 August 2012, Scheduled 6 September 2012*

* Corresponding author: Azzedine Bouaraba (abouaraba@gmail.com).

applied. Since SAR data contain amplitude and phase information, both parameters can be used as a change indicator [2]. The CCD technique detects a low-coherence area in the coherence map as changes [1, 3–5]. With the advent of high-resolution SAR images, CCD has received increased interest and new methods are now developed to enhance the change detection performance [5–9]. Unfortunately, the estimated coherence values are overestimated, especially for low coherence values. [4] investigates the accuracy of coherence estimation as a function of the coherence map resolution and demonstrates that the sample coherence magnitude estimator is biased especially for low coherence values. On the other hand, the lack of signal stationarity can be considered as a second source of bias for coherence estimation [10]. Recently, several methods have been proposed to enhance the coherence estimation. [6] proposes to use the degree of coherency and the excess of coherency factor to enhance change characterization. [7] presents a new method of interferometric phase flattening to improve the coherence between SAR images. This method can clarify the low coherence area due to terrain changes by improving coherence in the unchanged areas. [8] proposes a new algorithm to reduce several classes of false alarm from SAR CCD images. After the coherence improvement stage, a simple threshold applied to the coherence image may be used to distinguish between the changed and unchanged regions in the scene. [5] makes the assumption that, for X-band, man-made disturbances can cause potentially significant scatterer displacements, and hence a complete loss in coherence. By using CSK SAR images, [9] demonstrates that for all changed areas, caused by agricultural activities, the coherence is low but not completely lost, due to the presence of bias, especially for low values, in the coherence estimate [4], which considerably degrades the detection performance of the sample coherence thresholding method [9]. The bias decreases when the number of samples used to evaluate the coherence increases [4]. However, a large number of samples causes the loss of subtle changes in the coherence image. Furthermore, [4] proposes a method to reduce the bias, based on space-averaging coherence magnitudes over $M$-pixels local area. This method also allows the enhancement of the probability of detecting surface changes [9], but large window size is still needed to detect the entire changes. For that reason, another information source must be used to better analyze the coherence image. In repeat pass Interferometric SAR (InSAR), the phase difference (or interferogram) mainly displays the phase contribution related to the topography and the random phase which results from temporal changes. For some InSAR applications, not only the phase is of interest but also its local gradient, i.e., the Local

Fringe Frequencies (LFF) [11]. The LFF can be used in the InSAR processing at different stages, such as interferogram filtering [12] or phase unwrapping [13]. [10] also uses the LFF, as inputs to a speckle model, in order to reduce the coherence bias. [14] proposes a new method to estimate LFF components corresponding to low-resolution fringes and high-resolution patterns due to the local micro relief, respectively. The local phase slope is compensated, by using the estimated LFF components, to avoid the coherence bias due to the phase rotation within the estimation window. A careful analysis of the interferometric products, obtained with high resolution CSK data, reveals that the interferometric phase of changed areas is characterized by high LFF values (see Section 5). For an unchanged areas (i.e., without surface activity) the corresponding interferometric phase mainly consists of the topographic information with quite steady values, i.e., low LFF values. In the present paper, we use the LFF as additional information to clean coherence image in order to improve the performance of the existing coherence space-averaging method. The proposed method is based on using both range and azimuth LFF components to clean only highly coherent pixels inside changed areas, followed by the space-averaged coherence method. The probability of detection and false alarm are estimated experimentally using CSK images acquired in spot-light mode. The test site concerns fields with agricultural activities.

Our paper is organized as follows. Section 2 describes the interferometric coherence and the method of bias removal. Section 3 is dedicated to the LFF estimation. Section 4 presents the proposed method. Section 5 is devoted to the CCD application using CSK SAR data and to the evaluation of the change detection improvements obtained by the proposed method. A conclusion is given in the final section.

## 2. COHERENCE ESTIMATION AND BIAS REMOVAL

### 2.1. Interferometric SAR Coherence

The interferometric SAR coherence is evaluated in order to provide some measure of discrimination in the SAR image pair, and to accommodate the random noise fluctuations. Therefore, the sample complex cross correlation coefficient, between two SAR images $f$ and $g$, must be at first estimated as [4]:

$$\gamma_N = |\gamma_N| e^{j\phi} = \frac{\sum_{i=1}^{N} f_i g_i^*}{\sqrt{\sum_{i=1}^{N} |f_i|^2 \sum_{i=1}^{N} |g_i|^2}} \tag{1}$$

where $\gamma_N$ is the $N$-look complex coherence sample. The magnitude $|\gamma_N|$, namely called coherence, encodes the degree of scene similarity as a value in the range $[0, 1]$. The argument of $\gamma_N$, designed by $\phi$, is the interferometric phase which measures mainly both topography and any changes in the apparent radar range [5, 11]. As shown in [1, 5], the coherence may be expressed as the product of five dominant contributions:

**(i)** the relative backscatter signal to radar receiver noise ratio in the interferometric image pair,

**(ii)** the baseline decorrelation,

**(iii)** the volume decorrelation,

**(iv)** the decorrelation related to mismatch between primary and repeat-pass imagery, and

**(v)** the decorrelation caused by changes in the land surface, e.g., vegetation change or ploughing, which is the one in which we are interested.

If the repeat-pass imaging geometry is carefully designed and if the interferometric processing steps are performed correctly, it is possible to remove the effects of the first four contributions and retain only the fifth component. Man-made scene disturbance may be detected as areas of low coherence against undisturbed areas that are characterized by high values of coherence [5].

### 2.2. Coherence Bias Removal

A simple threshold applied to the coherence may be used to distinguish between the changed and unchanged regions in the scene. This method offers low-detection performance because of the presence of bias in the coherence estimate, especially for low coherence values [9]. In order to improve detection performance, the Mean Level Detector (MLD) can be applied by space-averaging coherence samples over $M$-pixels local areas [4]:

$$z_1 = \frac{1}{M} \sum_{i=1}^{M} |\gamma_{Ni}| \underset{H_1}{\overset{H_0}{\gtrless}} T_1 \tag{2}$$

where $M$ is the number of averaged coherence samples. $H_0$ is a realization of a null hypothesis (scene changes of interest are absent) and $H_1$ is the alternative hypothesis (scene changes of interest are present). To make a decision, the statistic $z_1$ is compared to a threshold $T_1$.

## 3. LOCAL FRINGE FREQUENCY ESTIMATION

Using 2-D notation, the complex InSAR phase of (1) can be modeled by a first-order approximation as (for simplicity, noise is neglected) [14]:

$$e^{j\phi(k,l)} = e^{j[2\pi(kf_x+lf_y)]} \tag{3}$$

where $f_x$ and $f_y$ are the LFF components respectively in range and azimuth directions. For ideal interferometric phase without noise, the fringe frequencies between adjacent pixels can be obtained as [15]:

$$f_x = (\phi(k+1,l) - \phi(k,l))/2\pi \tag{4}$$

$$f_y = (\phi(k,l+1) - \phi(k,l))/2\pi \tag{5}$$

From (1), the interferometric phase $\phi(k,l)$ includes all the frequencies components ($f_{xi}$, $f_{yi}$) that exist inside $N$-pixels local area. From (4) and (5), we see that LFF estimates can be obtained by differentiating the interferometric phase directly which is not limited by the first-order model [15]. Therefore, the measured interferometric phase is heavily influenced by noise. In this context, the LFF estimation can be realized by the maximum likelihood (ML) method [16] or by the modified multiple-signal classification (MUSIC) method [17]. In the present paper we use the MUSIC method, which offers better performance [17]. Note that the estimated LFF, over a small window-size, do not conflict with the real topography particularly when using high resolution SAR data.

## 4. PROPOSED METHODS OF CCD

In the available CSK high resolution SAR data, highly coherent pixels inside the changed area are clearly characterized by high LFF (see Section 5). In order to improve the CCD performances, the proposed method uses LFF as additional information to clean the coherence image as presented in Fig. 1.

To make use of the LFF, both in range and azimuth directions, we propose the following statistic:

$$z_2 = \frac{1}{2M}\sum_{i=1}^{M} |f_{xi}| + |f_{yi}| \gtrless T_2 \tag{6}$$

where $z_2$ represents an estimation of the interferometric phase variability inside a $M$-pixels local area. In CCD application, the topographic information is not the main concern and the number of samples $M$ is selected as small as possible to confer to $z_2$ the measurement of only terrain change. In the present work, the same

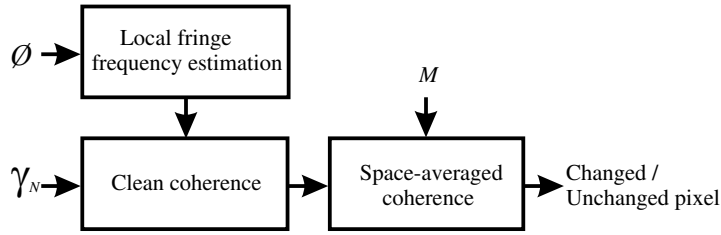


**Figure 1.** Scheme of the proposed method of CCD.

number of samples ($N = M = 3 \times 3$) were used for both coherence and $z_2$ estimation to preserve the high resolution of the data. The clean coherence step consists in the elimination of only highly coherent pixels (considered as aberrant values) inside changed areas. Therefore, the statistic $z_2$ must be compared to an appropriate threshold $T_2$. In case of $z_2$ exceeding the threshold value (case of high LFF value) the corresponding coherence value is set to 0. Otherwise (case of low LFF value) the coherence value remains unchanged. Finally, the cleaned coherence is space-averaged in order to improve the detection performance.

## 5. APPLICATION TO EXPERIMENTAL DATA

The results presented in this work are obtained with CSK data in X-band, horizontally polarized in spot-light mode. The CSK images are acquired on 1 and 9 January, 2010 with an incident angle of 41.5°. The pixel resolution is about 0.9 m in the ground range direction and 1 m in the azimuth direction. The test site, shown in Fig. 2, concerns fields with agricultural activities. The co-registration of the SAR images was performed with the SarscapeTM software (Sarmap 2012). Developments were carried out in IDL (Interactive Data Language). Figs. 3(a) and (b) show the magnitudes of the two used SAR images. With an acquisition period of eight days, the two images appear identical to the eye. On the other hand, the interferometric phase is more sensitive to the changes (see Fig. 2(c)). The coherence map, depicted in Fig. 3(d), shows several changed areas corresponding to cultivated parcels with low values of coherence. Coherence subsets have been geocoded and then projected in Google Earth to perform a comparison with high-resolution optical images (see Fig. 2). It had been verified that all areas with low values of coherence match perfectly boundaries of the agricultural parcels. By comparing the interferometric phase image to the coherence image shown in


**Figure 2.** Optical image from Google Earth. The test site in Maimana, Afghanistan, is characterized by a flat topography and crops. The rectangle indicates the area of interest corresponding to the used SAR images sub-set with a size of $1000 \times 1000$ pixels.

Fig. 3(d), we notice that for the changed area (red rectangle), the interferometric phase is uniformly distributed and is characterized by high local gradient values. For an unchanged area (blue rectangle) the interferometric phase consists mainly of the topographic information with quite steady values and low local gradient values. An analysis of Fig. 4 shows that the two histograms of $z_2$, corresponding to the selected changed and unchanged areas, are quite separated which confirms, in the case of real SAR data, that the proposed statistic $z_2$ represents an additional indicator of changes. In order to clean only highly coherent pixels inside the changed area, the statistic $z_2$ is compared to an appropriate threshold value $T_2$. In the present work, the value $T_2 = 0.2$ has been selected, which correspond to the intersection of the two histograms in Fig. 4. The cleaned coherence is then followed by space-averaging.

Receiver Operating Characteristics (ROC) curves have been used to quantify the detection performances of the proposed method. To evaluate experimentally ROC curves, changed and unchanged areas have been selected carefully as ground truth. The advantage of using high-resolution SAR data is that it is possible to select a large unchanged area ($90 \times 110$ pixels in the present work), characterized by a high-coherence mean value (about 0.85). The selection of changed area is easier in the case of SAR data in X-band as a subtle change

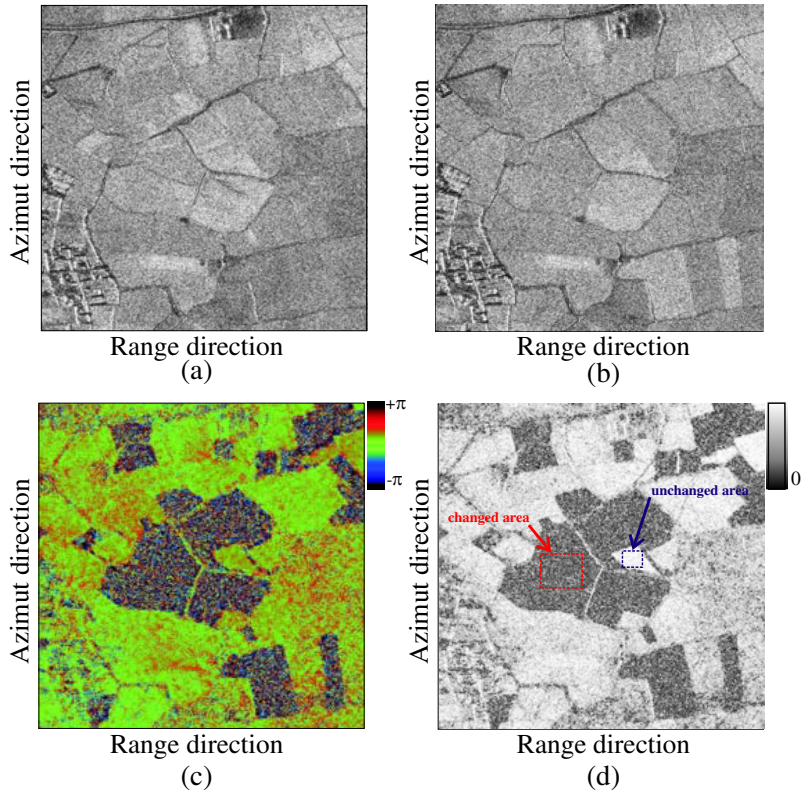


**Figure 3.** Cosmo-SkyMed SAR images and corresponding interferometric products. Sub-set size of 1000 × 1000 pixels. (a) Intensity of the complex SAR image of January 1, 2010. (b) Intensity of the complex SAR image of January 9, 2010. (c) Flattened and filtered interferometric phase. (d) Sample coherence evaluated using $N = 3 \times 3$ pixel spatial estimation window. Light-colored pixels represents values of coherence near 1, while dark pixels represent values near 0. The red rectangle shows the selected changed area (cultivated parcel with low coherence value) and the blue rectangle shows the selected unchanged area (undisturbed parcel with high coherence value). Cosmo-SkyMedTM Product-ASI [2010] processed under license from ASI-Agenzia Spaziale Italiana. All rights reserved.

on the terrain induces a decorrelation in the coherence image (see Fig. 3(d)). Here, the changed area has been chosen inside a field with agricultural activity (180 × 150 pixels sub-image). Fig. 5 depicts histograms of coherence images evaluated for different number $N$ of

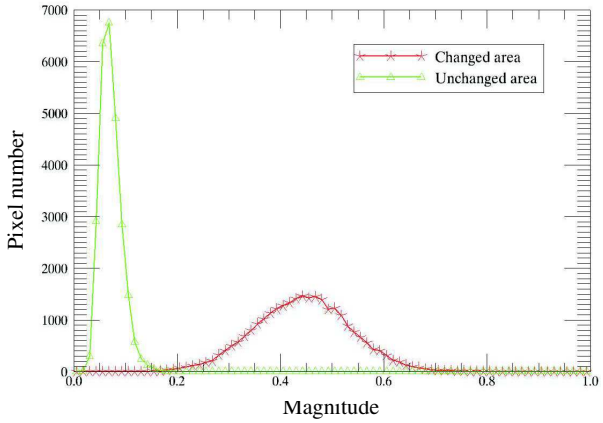


**Figure 4.** Histograms of the statistic $z_2$ in the selected changed and unchanged areas.

samples. It can be seen that the coherence bias induces the presence of highly coherent pixels in the changed area (light-colored pixels inside the changed area in Fig. 3(d)). The coherence bias decreases when increasing the number $N$ of samples used to estimate the coherence. For example, the coherence evaluated by using $N = 4 \times 4$ represents more faithfully the coherence of the changed area than the coherence evaluated by $N = 3 \times 3$, as there are less samples of high coherence inside the changed area. According to Fig. 5, the coherence mean value of the selected changed area is about 0.31 for $N = 4 \times 4$ against 0.41 for $N = 3 \times 3$. It is important to point out that coherence histograms of the changed area correspond to the same selected area and the discrepancy in the results is only due to the increasing number $N$ of samples. On the contrary, in case of the unchanged area, the coherence mean value is practically not affected by increasing the number $N$ of samples. According to Fig. 5, the coherence mean value of the unchanged area is about 0.85 for both $N = 3 \times 3$ and $4 \times 4$, which may be explained by the fact that the coherence estimate is particularly biased for the low coherence values. The analysis of Fig. 5 shows the necessity to increase the number $N$ of samples to obtain a good estimate of the coherence. But using high $N$ values also causes the loss of subtle changes in the coherence image. Therefore, the use of space-averaged coherences over $M$-pixels local area is required to enhance the change detection performances. In this context, the proposed method leads to an improvement of the space-averaged coherence method by using LFF as additional information. In the following paragraphs, we will attempt

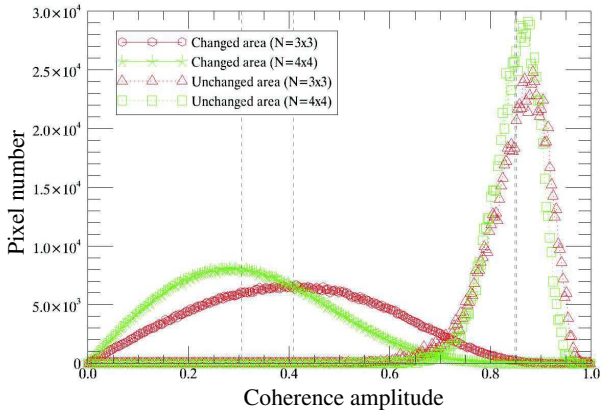


**Figure 5.** Histograms of the selected changed and unchanged areas coherences using different number $N$ of samples. The bias of coherence estimate, that affect particularly the low values, decreases with increasing $N$. The coherence mean value of the changed area is about 0.41 for $N = 3 \times 3$ and 0.31 for $N = 4 \times 4$. The coherence mean value of the unchanged area is about 0.85 for the different values of $N = 3 \times 3$ and $4 \times 4$.

to quantify this improvement in terms of probability of detection and false alarm. The detection performance may be quantified by evaluating the probability of detection $P_d$ and the corresponding false alarm rate $P_{fa}$ [5]:

$$P_d = \int_0^T P(\hat{\gamma}|\gamma = \gamma_{changed}) d\hat{\gamma} \tag{7}$$

$$P_{fa} = \int_0^T P(\hat{\gamma}|\gamma = \gamma_{unchanged}) d\hat{\gamma} \tag{8}$$

The procedure used to estimate experimentally $P_d$ and $P_{fa}$ is based on Equations (7) and (8). To evaluate $P_d$, the pixel under test is set in the middle of a moving window of size $M$, which is sliding to scan all coherence data of the selected changed area. The estimation of $P_d$ is then given by the ratio of the total number of times the test given by Equation (2) exceeds the threshold $T$ and the total number of data in the selected changed area. Similarly, the probability of false alarm $P_{fa}$ can be evaluated in the same way as $P_d$ by using the coherence data in the selected unchanged area. The estimation of $P_{fa}$ is then given by the ratio of the total number of times the test exceeds the threshold $T$ and the total number of data in the selected unchanged area. For low values of $T$, $P_{fa}$ is low, but $P_d$ will also be low and insufficient to detect all

changes. For high values of $T$, both $P_d$ and $P_{fa}$ will be high. Usually, we select a threshold that offers high (sufficient) $P_d$ and at the same time gives an acceptable false alarm rate. The ROC curves are defined as plots of $P_d$ versus $P_{fa}$ and are generated by varying the detector threshold $T$. Fig. 6 depicts the ROC curves evaluated for several values of $N$ and $M$. The ROC curve corresponding to $N = 3 \times 3$ and $M = 1$ offers the worst performances. Increasing the number $N$ of samples improves the detection performances. However, it also causes the loss of subtle changes in the coherence image. Substantial improvements may be obtained simply by space-averaging the coherence when using a window-size $M = 3 \times 3$. The proposed method offers a further improvement of about 6% of the detection probability when the false alarm rate is set to $P_{fa} = 10^{-3}$. This rate of false alarm is obtained with the simple thresholding method ($M = 1$) by using $N = 3 \times 3$ samples with a threshold value $T_1 = 0.73$, which corresponds to the intersection of changed and unchanged coherence histograms in Fig. 5. The CCD results corresponding to a false alarm rate of $P_{fa} = 10^{-3}$ are presented in Fig. 7. It can be noticed that the result of simple thresholding method ($M = 1$) of the coherence, see Fig. 7(a), is not usable ($P_d = 0.64$) due to the presence of a large number of highly coherent pixels inside the changed areas. An enhancement of the result is achieved by space-averaging coherence, see Fig. 7(b), by using a window of size $M = 3 \times 3$. In this case, the detection probability improves to $P_d = 0.94$ but remains insufficient. The best result is

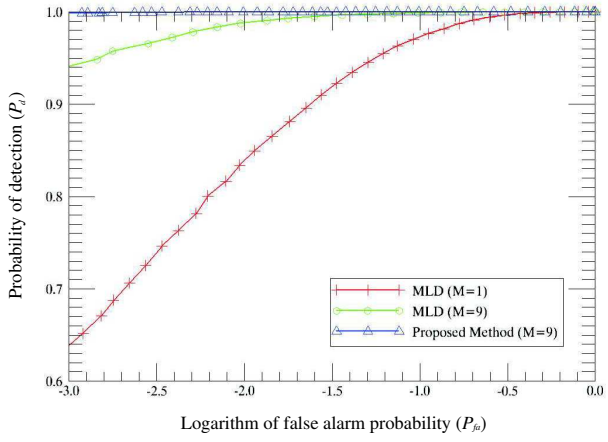


**Figure 6.** Experimental ROC curves corresponding to the acquisitions of January 1 and 9, 2010. Number of samples $N = 3 \times 3$. $T_2 = 0.2$.

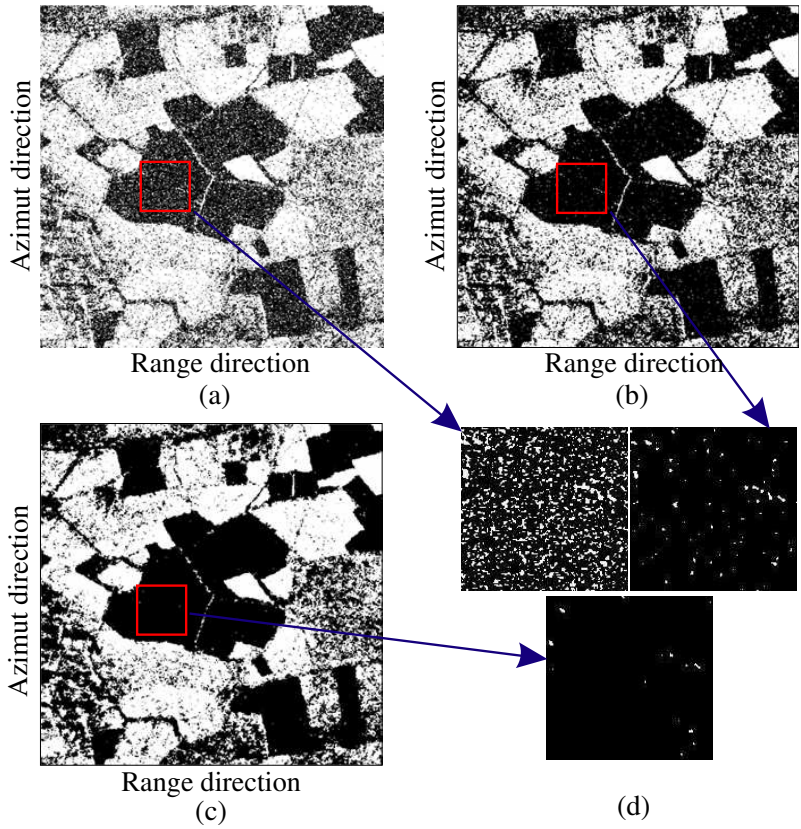


**Figure 7.** Coherent change detection results for $N = 3 \times 3$ and $P_{fa} = 10^{-3}$. (a) MLD change map with $M = 1$ and $P_d = 0.64$. (b) MLD change map with $M = 3 \times 3$ and $P_d = 0.94$. (c) Change map with the proposed method, $M = 3 \times 3$ and $P_d = 0.99$. (d) Zoom on a cultivated parcel.

obtained with the proposed method, as presented in Fig. 7(c), with a detection probability $P_d = 0.99$. In this case, the highly coherent pixels inside changed areas are mostly reduced (detection of almost all changes). The zoom of the changed area, as presented in Fig. 7(d), clearly indicates that the proposed method outperform the existing method MLD of CCD. The method had been successfully tested on another CSK pair images acquired on December 29 and 30, 2009. The results presented on Fig. 8 show that the method works also in steep terrain. The two cultivated parcels are almost detected, as showed in Fig. 8(d), even in area characterized by high values of topographic

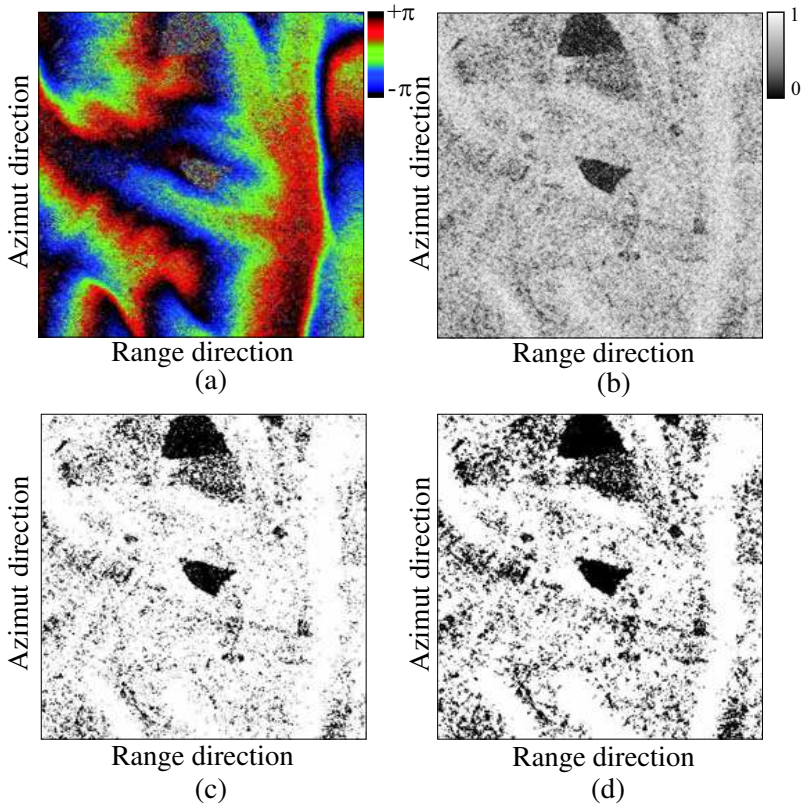


**Figure 8.** Interferometric results obtained by CSK SAR images acquired on December 29 and 30, 2009. Sub-set size of $1000 \times 1000$ pixels corresponding to a steep terrain. (a) Flattened and filtered interferometric phase. (b) Sample coherence evaluated using $N = 3 \times 3$ pixel spatial estimation window. (c) MLD change map with $M = 3 \times 3$, $P_{fa} = 10^{-3}$ and $P_d = 0.92$. (d) Change map with the proposed method, $M = 3 \times 3$, $P_{fa} = 10^{-3}$ and $P_d = 0.98$. Cosmo-SkyMedTM Product-ASI [2009] processed under license from ASI-Agenzia Spaziale Italiana. All rights reserved.

phase gradient. The limitation of the method can be noted in some situations where the phase contribution related to the topography is confined inside window-size of $3 \times 3$, which arrives rarely when using of high resolution SAR data. The method is also limited in case of low coherence values, such as forested area. The advantage of the proposed method is that it allows an enhancement of about 6% with respect to the coherence space-averaging method. In addition, this achieved by

using a small window size ($N = 3 \times 3$ and $M = 3 \times 3$) to preserve the detection of subtle changes.

## 6. CONCLUSION

In the present paper, a new CCD method based on the use of LFF's to clean coherence images is presented. To make use of the LFF both in range and azimuth directions, a new statistics that measures phase variability to eliminate the aberrant highly coherent pixels inside changed areas is proposed. The proposed method is tested successfully in the case of high resolution CSK SAR images acquired over fields with agricultural activities. The results show an improvement of the detection performances of about 6%, with respect to the method of space-averaging coherence while preserving the detection of subtle changes. The proposed method is an improvement for the analysts in charge of the vectorization of information derived from radar imagery inside a Geographical Information System.

## ACKNOWLEDGMENT

The Authors would like to thank the private companies Sarmap and EXELisvis for their support in providing a full SarscapeTM license (v.4.8, 2011) embedded in the latest version of ENVI software. The SAR data were obtained through a collaboration within NATO SET145 and processed at the Royal Military Academy of Belgium.

## REFERENCES

1. Zebker, H. A., "Decorrelation in interferometric radar echoes," *IEEE Trans. Geosci. Remote Sens.*, Vol. 30, No. 5, 950–959, 1992.
2. Rignot, E. J., "Change detection techniques for ERS-1 SAR data," *IEEE Trans. Geosci. Remote Sens.*, Vol. 31, No. 4, 896–906, 1993.
3. Corr, D. G., "Coherent change detection of vehicle movements," *Proc. IGARSS*, Vol. 5, 2451–2453, 1998.
4. Touzi, R., "Coherence estimation for SAR imagery," *IEEE Trans. Geosci. Remote Sens.*, Vol. 37, No. 1, 135–149, 1999.
5. Preiss, M., "Detecting scene changes using synthetic aperture radar interferometry," *IEEE Trans. Geosci. Remote Sens.*, Vol. 44, No. 8, 2041–2054, 2006.
6. Sabry, R., "A new coherency formalism for change detection and phenomenology in SAR imagery: A field approach," *IEEE Geosc. and Remote Sens. Letters*, Vol. 6, No. 3, 458–462, 2009.

7. Oishi, N., "A coherence improvement technique for coherent change detection in SAR interferometry," *Proc. of the 6th European Radar Conference*, Rome, Italy, Sep. 30–Oct. 2, 2009.
8. Phillips, R. D., "Clean: A false alarm reduction method for SAR CCD," *2011 IEEE Int. Conf. on Acoustics, Speech and Signal Processing (ICASSP)*, 1365–1368, May 2011.
9. Bouaraba, A., A. Younsi, A. Belhadj Aissa, M. Acheroy, N. Milisavljevic, and D. Closson, "Robust techniques for coherent change detection using Cosmo-SkyMed SAR images," *Progress In Electromagnetics Research M*, Vol. 22, 219–232, 2012.
10. Martinez, C. L., "Coherence estimation in synthetic aperture radar data based on speckle noise modeling," *Applied Optics*, Vol. 46, No. 4, 544–558, 2007.
11. Bamler, R., "Synthetic aperture radar interferometry," *Inverse Problems*, Vol. 14, No. 2, 1–54, 1998.
12. Lee, J. S., "Intensity and phase statistics of multilook polarimetric and interferometric SAR imagery," *IEEE Trans. Geosci. Remote Sens.*, Vol. 32, No. 5, 1017–1028, 1994.
13. Trouve, E., "Improving phase unwrapping techniques by the use of local frequency estimates," *IEEE Trans. Geosci. Remote Sens.*, Vol. 36, No. 6, 1963–1972, 1998.
14. Vasile, G., "High-resolution SAR interferometry: Estimation of local frequencies in the context of alpine glaciers," *IEEE Trans. Geosci. Remote Sens.*, Vol. 46, No. 4, 1079–1090, 2008.
15. Suo, Z., "A new strategy to estimate local fringe frequencies for InSAR phase noise reduction," *IEEE Trans. Geosci. Remote Sens. Lett.*, Vol. 7, No. 40, 771–775, 2010.
16. Spagnolini, U., "2-D phase unwrapping and instantaneous frequency estimation," *IEEE Trans. Geosci. Remote Sens.*, Vol. 33, No. 5, 579–589, 1995.
17. Trouve, E., "Fringe detection in noisy complex interferograms," *Applied Optics*, Vol. 35, No. 20, 3799–3806, 1996.